Heavy air pollution with a unique "non-stagnant" atmospheric boundary layer in the Yangtze River Middle Basin aggravated by regional transport of $PM_{2.5}$ over China

Chao Yu[1,2], Tianliang Zhao[1, *], Yongqing Bai[3, *], Lei Zhang[1,4], Shaofei Kong[5], Xingna Yu[1], Jinhai He[1], Chunguang Cui[3], Jie Yang[1], Yinchang You[1], Guoxu Ma[1], Ming Wu[1], Jiacheng Chang[1]

1 Collaborative Innovation Center on Forecast and Evaluation of Meteorological Disasters, Key Laboratory for Aerosol-Cloud-Precipitation of China Meteorological Administration, PREMIC, Nanjing University of Information Science and Technology, Nanjing 210044, China

2 Southwest Electric Power Design Institute Co., Ltd of China Power Engineering Consulting Group, Chengdu, 610021, China

3 Institute of Heavy Rain, China Meteorological Administration, Wuhan, 430205, China

4 Chengdu Academy of Environmental Sciences, Chengdu, 610031, China

5 Department of Atmospheric Sciences, School of Environmental Studies, China University of Geosciences (Wuhan), 430074, Wuhan, China

* *Correspondence*: Tianliang Zhao (tlzhao@nuist.edu.cn); Yongqing Bai (2007byq@163.com)

Abstract: The regional transport of air pollutants, controlled by emission sources and meteorological factors, results in a complex source-receptor relationship of air pollution change. Wuhan, a metropolis in the Yangtze River Middle Basin (YRMB) of Central China, experienced

heavy air pollution characterized by hourly $PM_{2.5}$ concentrations reaching 471.1 μg m^{-3} in January 2016. To investigate the regional transport of $PM_{2.5}$ over central-eastern China (CEC) and the meteorological impact on wintertime air pollution in the YRMB area, observed meteorological and other relevant environmental data from January 2016 were analyzed. Our analysis presented noteworthy cases of heavy $PM_{2.5}$ pollution in the YRMB area with unique "non-stagnant" meteorological conditions of strong northerly winds, no temperature inversion, and additional unstable structures in the atmospheric boundary layer. This unique set of conditions differed from the stagnant meteorological conditions characterized by near-surface weak winds, air temperature inversion, and stable structure in the boundary layer that are typically observed in heavy air pollution over most regions in China. The regional transport of $PM_{2.5}$ over CEC aggravated $PM_{2.5}$ levels, thus creating heavy air pollution in the YRMB area. This demonstrates a source-receptor relationship between the originating air pollution regions in CEC and the receiving YRMB region. Furthermore, a backward trajectory simulation using a FLEXPART-WRF model to integrate the air pollutant emission inventory over China was used to explore the patterns of regional transport of $PM_{2.5}$ governed by the strong northerly winds in the cold air activity of the East Asian winter monsoon season. It was estimated that the regional transport of $PM_{2.5}$ from non-local air pollutant emissions contributes more than 65% of the $PM_{2.5}$ concentrations to the heavy air pollution in the YRMB region during the study period, revealing the importance of the regional transport of air pollutants over China as a causative factor of heavy air pollution over the YRMB area.

Key words: $PM_{2.5}$ pollution; Yangtze River Middle Basin; meteorological condition; regional transport; FLEXPART-WRF

1. Introduction

Haze pollution can result in serious environmental problems that adversely influence human health, climate change, and other significant aspects (An et al., 2019; Fuzzi et al., 2015; Nel, 2005). Based on observations in China, there is a well-established association between haze pollution and high concentrations of $PM_{2.5}$ (particulate matter with an aerodynamic diameter equal to or less than 2.5 μm). Air pollution levels are highly dependent on the emissions of air pollutants and changes in meteorology (An et al., 2019; Tie et al., 2017; Xu et al., 2016a; Xu et al., 2016b). The accumulation, maintenance, and dissipation of haze pollution events are generally determined by meteorological changes (Zhang et al., 2013; Zhang et al., 2015), among which boundary layer structures play the most important role (Zhao et al., 2013). Meteorological conditions of stagnation, characterized by near-surface low winds, high humidity, and stable boundary layers, could govern the periodic variations of haze pollution, which present as typical wintertime air pollution in China (Huang et al., 2018; Xu et al., 2016b; Zhang et al., 2013). Major anthropogenic pollutant sources exist over the vast flatland in central-eastern China (CEC), from the eastern edges of the Tibetan Plateau and the Loess Plateau to China's Pacific coast. In the CEC, four major regions of emission sources that exhibit haze pollution with excessive $PM_{2.5}$ concentrations and overall poor air quality are centered over the North China Plain (NCP), the Yangtze River Delta (YRD) in East China, the Pearl River Delta (PRD) in South China, and the Sichuan Basin (SCB) in Southwest China. Over recent years, severe haze pollution events that have swept over much of CEC have been attributed to the regional transport of air pollutants (Cheng et al., 2008; Deng et al., 2011; Qiao et al., 2019; Tie et al., 2017; Wang et al., 2016; Zhang et al., 2012). The regional transport of air pollutants with a source-receptor relationship is an important issue in our

63 understanding of changes in air quality.

64 The source-receptor relationship of air pollution describes the impacts of emissions from
65 an upwind source region to pollutant concentrations or deposition at a downwind receptor area
66 (Seibert and Frank, 2004). The regional transport of source-receptor air pollutants is generally
67 complicated by two types of factors: emissions and meteorology (Voulgarakis et al., 2010; Zhao et
68 al., 2012). The emission factor includes emission source strength of air pollutants and the
69 precursors. Meanwhile, the meteorological factor determines the transport pathway from the
70 source to receptor regions, exchanges between the boundary layer and free troposphere, the
71 chemical transformation and the removal processes occurring over the source and receptor regions
72 as well as along the transport pathways. Driven by atmospheric circulations, the regional transport
73 of $PM_{2.5}$ from source regions can deteriorate air quality in the downwind receptor regions, leading
74 to the regional haze pollution observed in a large area over China (Chang et al., 2018; He et al.,
75 2017; Hu et al., 2018; Jiang et al., 2015; Wang et al., 2014).

76 The Yangtze River Middle Basin (YRMB) covers the lower subbasin of two provinces,
77 Hubei and Hunan, in Central China. It is geographically surrounded by four major haze pollution
78 regions, the NCP to the north, the YRD to the east, the PRD to the south, and the SCB to the west
79 (Fig. 1a). Due to the specialized location of the YRMB as a regional air pollutant transport hub
80 with subbasin topography (Fig. 1b), the regional transport of air pollutants driven by the cold air
81 flows of East Asian winter monsoon over CEC can create a special source-receptor relationship
82 between the source regions of haze pollution in upstream and the downwind YRMB region
83 (Zhong et al., 2019). However, there are unresolved questions regarding the meteorological

processes involved in the regional transport of air pollutants and the patterns of regional transport over CEC that may contribute to the air pollution changes observed in the YRMB area.

Wuhan, a metropolis located in the YRMB, has confronted environmental problems associated with urban air pollution, especially the heavy $PM_{2.5}$ pollution events that occur frequently in the winter (Gong et al., 2015; Xu et al., 2017). Local emissions of air pollutants from urban transportation, industrial exhaust, and bio-combustion play an important role in the YRMB urban air pollution (Acciai et al., 2017; Zhang et al., 2015). Previous observational and modeling studies on air pollution in this area have been conducted (Wu et al., 2018; Zheng et al., 2019). However, the regional transport routes of $PM_{2.5}$ across CEC are governed by meteorological drivers and their contribution to air pollution over the YRMB area are poorly understood, especially in relation to heavy air pollution events. This study selected Wuhan as a representative area within the YRMB for investigating the meteorological changes of air pollution events in January 2016 and assessing the contribution of regional transport of $PM_{2.5}$ over CEC to heavy air pollution in the YRMB area.

2. Data and methods

2.1 Data

Wuhan, the capital of the Hubei province, is located across the Yangtze River where its surrounding water network attributes to its humid environment (Fig. 1b). In order to analyze the air quality changes in Wuhan, hourly concentrations of air pollutants, including $PM_{2.5}$ in January 2016, were collected from the national air quality monitoring network operated by the Ministry of Ecology and Environment (http://www.mee.gov.cn/), including ten observational sites in Wuhan,

105 nine of which were urban sites in residential and industrial zones and one of which was suburban
106 (Fig. S1). The air quality observation data are released by the Ministry of Ecology and
107 Environmental Protection under quality control that is based on China's national standard of air
108 quality observation.

109 The meteorological data of surface observations and air sounding in Wuhan and other
110 observatories in CEC were obtained from the Meteorological Data Sharing Network of China
111 Meteorological Administration (http://data.cma.cn/). The data selected for this study included air
112 temperature, relative humidity, air pressure, and wind speed and wind direction. In order to
113 analyze the meteorological variations in the atmospheric boundary layer at the time of our study,
114 we used data with temporal resolutions of 3 h for surface observations, and 12 h for sounding
115 observations.

116 The surface $PM_{2.5}$ concentrations, averaged over the ten observational sites in Wuhan, were
117 used to characterize the variations of air pollution in January 2016 over this urban area.
118 Correlation coefficients were calculated between the 10-site averages and the observed
119 meteorological elements, including wind speed and air temperature, in Wuhan to explore the local
120 meteorological influences on the changes of ambient $PM_{2.5}$ concentrations.

121 The ERA-Interim reanalysis data from the European Centre for Medium-Range Weather
122 Forecasts (ECMWF) (https://www.ecmwf.int/en/forecasts/datasets/reanalysis-datasets/) were
123 applied to explore the cold air flows of East Asian winter monsoonal winds in January 2016 and
124 their anomalies during heavy $PM_{2.5}$ pollution over CEC.

2.2 FLEXPART-WRF modeling

2.2.1 Model description

The Flexible Particle dispersion (FLEXPART) model (Stohl et al., 2003; Stohl et al., 2005) is a Lagrange particle diffusion model developed by the Norwegian Institute for Air Research (NIAR). In this model, the trajectory of a large number of particles released from a source is simulated, considering the processes of tracer transport, turbulent diffusion, and wet and dry depositions in the atmosphere (Brioude et al., 2013). Applying a backward trajectory simulation can determine the distribution of potential source regions that may have an impact on a target point or receptor region (Chen et al., 2017a; Chen et al., 2017b; Seibert and Frank, 2004; Zhai et al., 2016).

Initially, the FLEXPART model could be driven by the global reanalysis meteorological data obtained from the ECMWF or the National Centers of Environmental Prediction (NCEP). However, since this study focuses on the fine and multiscale modeling of air pollutant sources and regional transport, the FLEXPART model was driven by the Weather Research and Forecasting (WRF) model to effectively devise the combined model FLEXPART-WRF (Fast and Easter, 2006; Brioude et al., 2013), which has been widely used to investigate the potential sources of air pollutants regarding environmental change (An et al., 2014; De Foy et al., 2011; Sauvage et al., 2017; Stohl et al., 2003).

2.2.2 WRF modeling configuration and meteorological validation

In this study, the WRF model was configured with two nested domains, coarse and fine. The coarse domain covered the entirety of Asia with a 30 × 30 km horizontal resolution, and the nested

fine domain included most of China and its surrounding regions with a 10 × 10 km horizontal resolution (Fig. S2). The physical parameterizations used in WRF modeling were selected with the Morrison microphysics scheme (Morrison et al., 2009), the Rapid Radiative Transfer Model (RRTM) scheme for long and short wave radiation (Mlawer et al., 1997), the Yonsei University (YSU) boundary layer scheme (Hong et al., 2006), the Grell 3D cumulus parameterization, and the Noah land surface scheme (Grell et al., 2005). Using the reanalysis meteorological data in the horizontal resolutions of 1°×1° obtained from NCEP for initial and boundary meteorological conditions, the WRF simulation ran 12 h each time, where the first 6 h simulations constituted spin-up time.

The WRF-simulated meteorological fields, which included wind speed and direction, air temperature, relative humidity, and air pressure, were compared with observations at five typical sites (Wuhan, Changsha, Hefei, Zhengzhou, and Nanchang) over CEC (Fig. 2). The correlation coefficients were calculated and found to pass the significance level of 0.001, and the normalized standardized deviations were determined to be low (Taylor, 2001) (Fig. 2). Based on these results, it was evaluated that the WRF modeled meteorology was reasonably consistent with observations and could be used to drive the FLEXPART backward trajectory simulation.

2.3 Estimating contribution of regional transport of $PM_{2.5}$ to air pollution

In the FLEXPART-WRF model, the trajectory of particles released from a source is simulated. Using this Lagrangian method could result in a Jacobian matrix (footprint) with units of mass per volume per unit flux. Stohl et al (2005) mathematically derived the residence time for particles out of FLEXPART. Generally, in the backward trajectory of FLEXPART modeling, many particles are

167 released at a receptor and transported backward in time. Then the residence time (not the lifetime)
168 of all particles, normalized by the total number of released particles, is determined on a uniform
169 grid. Selecting Wuhan as the receptor in the YRMB, the residence time for a thickness of 100 m
170 above the surface was calculated and considered as the ‘‘footprint’’ (in units of s). By multiplying
171 the residence time with the air pollutant emission flux in the respective grid cell (in units of μg m^{-2}
172 s^{-1}) calculated from the air pollutant emission inventory of 2016 for China
173 (http://www.meicmodel.org/), the emission source contribution (in units of μg m^{-2}) from this grid
174 cell to the receptor’s air pollution change could be estimated (Stohl et al., 2003; Stohl et al., 2005;
175 Ding et al., 2009).

176 In this study, the FLEXPART-WRF simulation was conducted for a 48-hour backward
177 trajectory with the release of 50,000 air particles in the first h from Wuhan (30.61°N, 114.42°E)
178 for three heavy pollution events in January 2016. The results were output with the residence time
179 of air particles in a horizontal resolution of 0.1° × 0.1°. The simulations of particle residence time
180 over the 48 h backward trajectory pathways were multiplied with the regional primary $PM_{2.5}$
181 emission fluxes to quantify the contribution of regional transport of $PM_{2.5}$ to air quality change in
182 the YRMB area while identifying patterns of regional transport of $PM_{2.5}$ over CEC. The primary
183 $PM_{2.5}$ emission data from the Multi-resolution Emission Inventory for China (MEIC)
184 (http://www.meicmodel.org/) in 2016 were selected for use as the regional $PM_{2.5}$ emission fluxes
185 in this study.

186 Based on this backward trajectory simulation, the upstream sources of $PM_{2.5}$ emissions for
187 heavy air pollution in Wuhan were identified. The contribution rates $\boldsymbol{rate_{i,j}}$ of regional transport of
188 $PM_{2.5}$ from the upstream sources to air pollution in the downstream receptor region of the YRMB

were calculated by Eq. (1), and the total contribution ***R*** of regional transport from the non-local emission sources are estimated by Eq. (2) (Chen et al., 2017b; Ding et al., 2009).

$$rate_{i,j} = \frac{E_{i,j} \times r_{i,j}}{\sum_{1,1}^{N,S} E_{i,j} \times r_{i,j}} \qquad (1)$$

$$R = \sum_{(N_1,S_1)}^{(N_2,S_2)} rate_{i,j} \qquad (2)$$

where the subscripts ***i*** and **j** represent a grid location (***i, j***) over the 48 h backward trajectory from the first grid (***i***=1, ***j***=1) in Wuhan to the last grid (***i***=*N*, ***j***=*S*) over CEC; $\mathbf{r}_{i,j}$ represents the residence time of $PM_{2.5}$ particles simulated by FLEXPART-WRF; and $E_{i,j}$ represents the $PM_{2.5}$ emission flux over the grid. In Eq. (2), the first grid location (N_1, S_1) and the last grid location (N_2, S_2) over the non-local emission sources and the local area of Wuhan were determined, respectively, by the regional transport of $PM_{2.5}$ pathways and the YRMB area in Wuhan as simulated by the FLEXPART-WRF model.

3. Results and Discussion

3.1 Variations in local $PM_{2.5}$ concentrations and meteorology in January 2016

Based on the National Ambient Air Quality Standards of China released by the Ministry of Ecology and Environment in 2012 (http://www.mee.gov.cn/), light and heavy air pollution levels of $PM_{2.5}$ are categorized by the daily average $PM_{2.5}$ concentrations exceeding 75 and 150 μg m^{-3} in ambient air, respectively. The average monthly $PM_{2.5}$ concentration reached 105.8 μg m^{-3} in Wuhan, where the daily $PM_{2.5}$ concentrations exceeded 75 μg m^{-3} on 27 days during the entire month of January 2016 (Fig. 3a), indicating that this YRMB urban area was under significant $PM_{2.5}$ pollution during this wintertime period. As shown in Figure 3a, a 21 day prolonged air

pollution event resulted from high levels of daily $PM_{2.5}$ concentrations (> 75 μg m^{-3}) from the 1st to the 21st. During this period, three notably heavy air pollution events occurred on January 4th, the 10th to the 12th, and the 17th to the 18th with excessive daily $PM_{2.5}$ concentrations (>150 μg m^{-3}). These three events are marked as P1, P2, and P3, respectively (Fig. 3b). Based on these observations, we found the interesting phenomenon of an approximately 7 day cycle of heavy air pollution, reflecting an important modulation of meteorological oscillation in the East Asian winter monsoonal winds affecting air pollution over the YRMB region (Xu et al., 2016a). A period analysis on long-term observation data of air quality could provide further understanding on air quality changes associated with meteorological drivers.

Figure 3b presents the hourly changes of $PM_{2.5}$ concentrations during the three heavy air pollution events P1, P2, and P3. P1 began at 11:00 a.m. (local time is used for all events) and ended at 11:00 p.m. the same day with an observed $PM_{2.5}$ concentration peak of 471.1 μg m^{-3}. P2 occurred from 10:00 p.m. on the 10th to 00:00 a.m. on the 12th. Over the 26 hour duration, it had two peaks: 231.4 and 210.6 μg m^{-3}. P3 occurred between 7:00 p.m. on the 17th and 2:00 p.m. on the 18th with an explosive growth rate of 42.9 μg m^{-3} h^{-1}. These events were characterized by short durations of less than 26 h from rapid accumulation to fast dissipation.

The changes in $PM_{2.5}$ concentrations presented few differences between the suburban and urban sites. Both had similar patterns and peaks of hourly changes during the heavy pollution periods (Figs. S3, S4, and S5), demonstrating that regional heavy air pollution in a large area of the YRMB region is, in part, due to regional transport over CEC. The only obvious differences in air pollutant concentrations were measured during the clean air periods ($PM_{2.5}$ concentration < 75 μg m^{-3}) with the relatively high and low concentrations of $PM_{2.5}$ at urban and suburban sites,

230 respectively (Figs. S3, S4, and S5). This shows the important influence of high air pollutant
231 emissions over urban areas on local air quality.

232 Using the environmental and meteorological data observed in Wuhan in January 2016, the
233 effects of the meteorological conditions on $PM_{2.5}$ concentrations in the YRMB region were
234 statistically analyzed in regard to hourly variations of surface $PM_{2.5}$ concentrations, near-surface
235 wind speed (WS), wind direction (WD), surface air temperature (T) and pressure (P), and relative
236 humidity (RH) (Fig. 4). Among the observed changes shown in Figure 4, the changes of $PM_{2.5}$
237 concentrations were found to have obviously positive correlations to T and RH, as well as a
238 pronounced negative correlation to P and a weak positive correlation to WS (Table 1). There are
239 several reasons for these results. Firstly, the lower WS could alter the concentrations of air
240 pollutants with a weaker advection of cold air in conjunction with strong subsidence and stable
241 atmospheric stratification, thus easily producing a stagnation area in the lower troposphere and
242 resulting in regional pollutant accumulations for the development of haze events. Secondly, in the
243 presence of high soil moisture, strong surface evaporation could increase the near-surface RH,
244 which is conducive to the hygroscopic growth of participles for haze formation (Dawson et al.,
245 2014; Xu et al., 2016a). Additionally, high air temperature and strong solar radiation could
246 enhance chemical conversions for the formation of secondary aerosols in the atmosphere (He et al.,
247 2012; Huang et al., 2014). Furthermore, precipitation could impact the emissions of fugitive dust
248 and depositions of air pollutants (Dawson et al., 2007; Cheng et al., 2016). These observations
249 could reflect the special influences of meteorological factors, such as winds, air temperature,
250 humidity, and precipitation, on the physical and chemical processes in the ambient atmosphere that
251 affect air quality change in the YRMB region.

3.2 A unique meteorological condition of "non-stagnation" for heavy $PM_{2.5}$ pollution

3.2.1 Strong northerly winds

When we focused on the meteorological changes leading to high $PM_{2.5}$ levels exceeding 150 μg m^{-3} during the heavy air pollution events, it is noteworthy that all three episodes, P1, P2, and P3, were accompanied with strong WSs in the northerly direction, as well as evident turning points in prevailing conditions leading to falling T and increasing P (Fig. 4). The conditions observed during these episodes present the typical meteorological characteristics of cold air invasion with high air pressure over the East Asian monsoon region. The southward advance of a cold front could drive the regional transport of air pollutants over CEC (Kang et al., 2019). Climatologically, a strong northerly wind, low air temperature, and high air pressure are typical features of an incursion of cold air during the East Asian winter monsoon season that could disperse air pollutants, thus improving air quality in the NCP region (Miao et al., 2018; Xu et al., 2016b). This differs from the meteorological conditions of stagnation with weak winds observed for heavy air pollution events in the major air pollution regions of CEC (Ding et al., 2017;Huang et al., 2018), and the strong near-surface wind that anomalously accompanied the intensification of $PM_{2.5}$ during heavy air pollution periods over the study area (Fig. 4). This could imply that the regional air pollutant transport is worsening air quality over the YRMB, driven by the strong northerly winds during the East Asian winter monsoon season.

To further investigate the connection between meteorological elements in the near-surface layer and changes in air quality affected by $PM_{2.5}$ concentrations in the YRMB region, we carried

out a more detailed correlation analysis of $PM_{2.5}$ concentrations in Wuhan with WS and air temperature for three different levels of $PM_{2.5}$ concentrations: clean air environment ($PM_{2.5} < 75$ μg m^{-3}), light air pollution (75 μg $m^{-3} \leq PM_{2.5} < 150$ μg m^{-3}) and heavy air pollution ($PM_{2.5} \geq 150$ μg m^{-3}) periods (Table 2). The surface $PM_{2.5}$ concentrations were positively correlated with air temperature, and negatively correlated with wind speeds during the periods of clean air environment and light air pollution. It should be emphasized here that a significantly negative correlation (R = -0.19) of $PM_{2.5}$ concentrations to WS for the light air pollution period could indicate that weak winds are favorable for local $PM_{2.5}$ accumulation, reflecting an important effect of local air pollutant emissions on light air pollution periods over the YRMB area. In January 2016, the overall wind speed of Wuhan was weak with a monthly mean value of 2.0 m s^{-1}, which could help maintain the high $PM_{2.5}$ levels in the prolonged air pollution events experienced in the YRMB area. However, a significantly positive correlation (R = 0.41) existed between heavy air pollution levels of $PM_{2.5}$ concentrations ($PM_{2.5} > 150$ μg m^{-3}) and strong WSs during the heavy air pollution periods, which was inconsistent with the meteorological conditions of stagnation observed in the near-surface layer where weak winds were associated with heavy air pollution in East China (Cao et al., 2012; Deng et al., 2011). The meteorology and environment conditions in the YRMB region indicate the close association of heavy air pollution periods enhancing $PM_{2.5}$ concentrations with strong winds (Fig. 4, Table 2), therefore, reflecting a key role of regional transport of air pollutants in the development of the YRMB's heavy air pollution periods.

In order to clearly illustrate the impact of wind speed and direction on the $PM_{2.5}$ concentrations associated with the regional transport of upwind air pollutants, Figure 5 presents the relation of hourly changes in surface $PM_{2.5}$ concentrations to WS and wind direction in Wuhan

during January 2016. As seen in Figure 5, strong northerly winds accompanied extremely high $PM_{2.5}$ concentrations (> 150 μg m^{-3}) during the heavy air pollution periods, including a northeast gale exceeding 5 m s^{-1} during the extreme heavy pollution periods with extremely high $PM_{2.5}$ concentrations (> 300 μg m^{-3}). These results reveal a unique meteorological condition of "non-stagnation" with strong winds during events of heavy air pollution over the YRMB area. Conversely, the observed $PM_{2.5}$ concentrations ranging between 75 and 150 μg m^{-3} for light air pollution periods generally corresponded with low wind speeds (< 2 m s^{-1}) (Fig. 5). Therefore, it is the meteorological condition of stagnation, characterized by weak winds, involved in the accumulation of local air pollutants that is responsible for the light air pollution periods. Meteorological impacts on air quality could include not only the stagnant condition of meteorology with weak winds and stable boundary layer but also air temperature, humidity, precipitation, and atmospheric radiation in close connection with atmospheric physical and chemical processes. The meteorological drivers of air quality change are complicated by a series of physical and chemical processes in the atmosphere, especially the formation of secondary air pollutants with strong hygroscopic growth in the humid air environment overlying the dense water network (Fig. 1b) in the YRMB region (Cheng et al., 2014; He et al., 2012; Huang et al., 2014).

3.2.2 Unstable structures in the atmospheric boundary layer

The air sounding data observed in Wuhan were used to compare the structures of the atmospheric boundary layer during the heavy air pollution and clean air periods. Figure 6 presents the vertical profiles of air temperature, wind velocity, and potential temperature averaged for the heavy $PM_{2.5}$ pollution and clean air periods in January 2016. It can be seen that the inversion layer of air temperature did not exist during the heavy pollution periods, while a near-surface inversion

317 layer appeared at the height of about 200 m during the clean air periods (Fig. 6a). Compared to the
318 clean air period, the heavy air pollution events had stronger winds within the 1000 m layer but
319 weaker winds above the 1000 m layer (Fig. 6b), indicating that the regional transport of $PM_{2.5}$ was
320 mainly limited to the 1000 m layer, especially between 250 m and 800 m. These vertical structures
321 of horizontal wind could conduce to the downward mixing of the regionally transported air
322 pollutants and produce the near-surface accumulations of air pollutants over the YRMB area with
323 elevated ambient $PM_{2.5}$ concentrations, thus contributing to heavy air pollution.

324 To quantitatively characterize the stability of the atmospheric boundary layer, the vertical
325 profiles of potential air temperature (θ) were calculated with air temperature and pressure (Fig. 6c).
326 In this study, the vertical change rate of θ was used to quantify the static stability of the boundary
327 layer (Oke, 2002). A lower vertical change rate of θ generally indicates decreasing stability or
328 increasing instability of the boundary layer. The averaged static stability values of the near-surface
329 layer below a height of 200 m during the heavy pollution and clean air periods were
330 approximately 4.4 and 13.2 K km^{-1}, respectively (Table 3). This obvious decrease in stability of
331 the boundary layer from clean air to heavy pollution periods indicates an anomalous tendency of
332 the unstable boundary layer for the heavy pollution periods during January 2016 in the YRMB
333 area.

334 The meteorological conditions of stagnation characterized by weak wind, temperature
335 inversion, and a stable vertical structure of the atmospheric boundary layer are generally accepted
336 as the typical meteorological drivers for heavy air pollution (An et al., 2019; Ding et al., 2017).
337 Nevertheless, this study revealed a unique meteorological condition of “non-stagnation” in the
338 atmospheric boundary layer during heavy air pollution periods characterized by strong wind, lack

of an inversion layer, and a more unstable structure of the atmospheric boundary layer. These "non-stagnant" meteorological conditions could be generally regarded as the typical pattern of atmospheric circulation that facilitates the regional transport of air pollutants from upstream sources to downwind receptor regions. The regional transport of $PM_{2.5}$ connected with the source-receptor relationship between the air pollution regions in CEC and the YRMB area was further investigated with the following observational and modeling analyses.

3.3 Regional transport of $PM_{2.5}$ in northerly winds observed over CEC

The monthly averages of $PM_{2.5}$ concentrations and the anomalies of wind speed averaged in three heavy air pollution periods relative to the monthly mean wind speed in January 2016 observed over CEC are shown in Figure 7. Note that a large area of CEC experienced air pollution with high levels of $PM_{2.5} > 75$ μg m^{-3} that were especially severe in the NCP region and the Fenhe-Weihe Plain in Central China (Fig. 7a). As seen in Figure 7, Wuhan (site 1 in Fig. 7a) and the surrounding YRMB region were situated in the downwind southern edge of the air pollution area blanketing CEC (Fig. 7a), where the northerly winds prevailed (Fig. 7b). Climatologically, CEC is a typical region of East Asian monsoons dominated with wintertime northerly winds (Ding, 1993). Note that the anomalously stronger northerly winds were observed over upstream CEC during the three periods of wintertime heavy $PM_{2.5}$ pollution (Fig. 7b). Driven by the stronger northerly winds, the regional transport of air pollutants from the source regions in windward CEC could largely contribute to heavy air pollution in the downwind receptor region of YRMB.

In order to explore the connection between the regional transport of $PM_{2.5}$ over CEC and the three events of heavy air pollution in the YRMB region, six observational sites were selected from

360 the northwestern, northern, and northeastern directions over upstream CEC (Fig. 7a). These sites
361 represent three different routes of the regional transport of $PM_{2.5}$ to Wuhan (site 1 in Fig. 7a) and
362 are governed by the southward incursion of stronger northerly winds (Fig. 7b). Figure 8 presents
363 the temporal changes of $PM_{2.5}$ concentration and wind speed along three typical routes of regional
364 transport of $PM_{2.5}$ over CEC. The southeastward movement of heavy $PM_{2.5}$ pollution was driven
365 by stronger northerly winds from Luoyang and Xinyang to Wuhan (sites 3, 2, and 1 in Fig. 7) and
366 presented a northwestern route of regional transport of $PM_{2.5}$ for P1 (see upper panels of Fig. 8).
367 The westward advance of $PM_{2.5}$ peaks was governed by the northeastern winds from Tongling and
368 Hefei to Wuhan (sites 6, 5, and 1 in Fig. 7a). The regional transport of $PM_{2.5}$ across Eastern China
369 to the YRMB in Central China exerted a significant impact on P2 (see middle panels of Fig. 8). A
370 northern pathway of regional transport of $PM_{2.5}$ connected Zhengzhou and Xinyang to Wuhan
371 (sites 4, 2, and 1 in Fig. 7a) during P3 with anomalously strong northerly winds (see Fig. 7b and
372 lower panels of Fig. 8). Note, in Figure 8, that the heavy $PM_{2.5}$ pollution periods at the upstream
373 sites of Hefei, Tongling, Luoyang, Xinyang, and Zhengzhou (sites 2-6 in Fig. 7a) were generally
374 dispelled by strong northerly winds. At the same time, these winds could trigger the periods of
375 heavy $PM_{2.5}$ pollution in the YRMB region (Wuhan, site 1 in Fig. 7a). Such inverse effects of
376 strong winds on heavy air pollution in CEC and the YRMB region show the important role that
377 regional transport of air pollutants can have in cleaning and worsening air pollution in the
378 upstream CEC source regions and the downstream YRMB receptor region, respectively.

379 The regional transport over CEC that is associated with the source-receptor relationship
380 directing heavy $PM_{2.5}$ pollution to the YRMB region was revealed via observational analysis. The
381 FLEXPART-WRF backward trajectory modeling was used to further identify the patterns of

382 regional transport of $PM_{2.5}$ and estimate the resulting contribution to heavy air pollution in the
383 YRMB region in the following section.

384 3.4 Contribution of regional transport of $PM_{2.5}$ to heavy pollution

385 In this study, for the receptor of Wuhan, the $PM_{2.5}$ contributions of regional transport over
386 CEC to air pollution in the downwind receptor region could be approximately estimated. These
387 estimations were based on the product of the residence time of air particles during regional
388 transport as simulated by the FLEXPART-WRF model, and the $PM_{2.5}$ emission flux over the
389 source grid in CEC determined by Eq. (1). The data yielded a so-called potential source
390 contribution map, which is the geographical distribution of the regional transport contribution
391 rates (%) of the emission source grid cell to $PM_{2.5}$ pollution at the receptor of Wuhan (Fig. 9).

392 The non-local emission sources that affected $PM_{2.5}$ concentrations during P1, P2, and P3
393 were quantified over CEC using the $PM_{2.5}$ contribution rates calculated with Eq. (1). Combining
394 the distribution of high $PM_{2.5}$ contribution rates with the prevailing winds experienced during the
395 three heavy $PM_{2.5}$ pollution periods, the major pathways of regional transport of $PM_{2.5}$ over CEC
396 could be recognized (Fig. 9). During P1 in the YRMB region, the regional transport of air
397 pollutants was centered along a northwestern route from the Fenhe-Weihe Plain in Central China,
398 and a northeastern route from the YRD region in Eastern China (Fig. 9a). The YRD emission
399 sources of air pollutants exerted a large impact on P2 through regional transport of $PM_{2.5}$ across
400 Eastern China to the YRMB region along the north side of Yangtze River (Fig. 9b). Two major
401 regional transport pathways of $PM_{2.5}$ indicated by the spatial distribution of high contribution rates
402 of $PM_{2.5}$ from the NCP and YRD regions contributed to the elevated $PM_{2.5}$ concentrations during

403 P3 (Fig. 9c). Governed by the anomalous northerly winds in January 2016 (Fig. 7b), the regional
404 transport of $PM_{2.5}$ from the air pollutant emission source regions in CEC provided a significant
405 contribution to the wintertime heavy $PM_{2.5}$ pollution observed in the YRMB region (Figs. 7-9).
406 This was confirmed by the results of the FLEXPART-WRF backward trajectory simulation
407 utilized in this study.

408 The $PM_{2.5}$ contributions of regional transport over CEC to the $PM_{2.5}$ concentrations in the
409 YRMB area during P1, P2, and P3 were estimated using Eq. (2) with the resulting high
410 contribution rates of 68.1%, 60.9%, and 65.3%, respectively (Table 4). The regional transport of
411 $PM_{2.5}$ from non-local air pollutant emissions could contribute more than 65% of the $PM_{2.5}$
412 concentrations to the heavy air pollution in the YRMB region during the study period, revealing a
413 large contribution of regional transport of $PM_{2.5}$ over CEC to the enhancement of $PM_{2.5}$ levels in
414 the YRMB area for the wintertime heavy air pollution.

415 Note that the potential source contribution is estimated based on transport alone, ignoring
416 chemical and removal processes. We understand that these processes, including complex
417 deposition, and chemical conversion for the formation of secondary particles, were not introduced
418 in the FLEXPART-WRF simulation, which could represent the basic features of contribution and
419 patterns of regional $PM_{2.5}$ transport over CEC when limited to the primary $PM_{2.5}$ particles
420 highlighted in this study.

421 Normally researchers rely on 3-D numerical models with process analysis capability, such
422 as integrated process rates (IPRs), in order to quantify the contributions of regional transport to the
423 occurrence of air pollution episodes (Gao et al., 2011; Hu et al., 2018; Jiang et al., 2015). In this

study, simulations with a Lagrange particle dispersion FLEXPART-WRF model were utilized to calculate the percentage contribution of regional transport while identifying the transport pathway. The major uncertainty of this method for such calculations, as compared to other methods such as IPRs, is that the physical and chemical processes, including chemical conversion for the formation of secondary particles, were not introduced in the FLEXPART-WRF simulation. Considering that there is less precipitation in the winter monsoon season over CEC, this methodology has proven its robustness to quantify the regional transport contribution within the uncertainty range by relying on a portion of secondary organic and inorganic aerosols that resulted from the complex physical and chemical processes in the atmosphere.

4. Conclusions

This study investigated the ambient $PM_{2.5}$ variations over Wuhan, a typical YRMB area in Central China in January 2016, by analyzing the observational data of the environment and meteorology. In addition to this, we did a FLEXPART-WRF simulation to explore the meteorological processes involved in the regional transport of air pollutants, the regional transport patterns of $PM_{2.5}$, and how it contributes to heavy air pollution in the YRMB region. Focusing our study on three heavy $PM_{2.5}$ pollution periods we found a unique “non-stagnant” atmospheric boundary layer for wintertime heavy air pollution that was aggravated by the regional transport of $PM_{2.5}$ over CEC. This boundary layer was characterized by strong winds, no inversion layer, and a more unstable structure. These non-stagnant conditions during heavy air pollution periods with high $PM_{2.5}$ concentrations facilitate our understanding of the air pollutant source-receptor relationship of regional transport in air quality change. Our study is of great interest to the air quality community given the unique features of the air pollution meteorology, which are very

different from “stagnant” meteorological conditions presented in textbooks.

Although emissions and local accumulation of air pollutants can lead to the formation of light air pollution, in regard to $PM_{2.5}$ over the YRMB region, the regional transport of $PM_{2.5}$ from upstream source regions of air pollutant emissions in CEC contributed significantly (more than 65%) to the excessive $PM_{2.5}$ concentrations during wintertime heavy air pollution in the downwind YRMB region in January 2016, as governed by the strong northerly winds in the East Asian winter monsoon season over CEC.

Based on the variations of air quality and meteorology in a typical urban YRMB region, this study revealed a unique “non-stagnant” meteorological condition for heavy air pollution with a strong contribution of regional transport of $PM_{2.5}$ over China. These conditions and contributions can be investigated further with climate analyses of long-term observations and more comprehensive modeling of air quality and meteorology.

Data availability: The data used in this paper can be provided by Chao Yu (ychao012@foxmail.com) upon request.

Supplement: The supplement related to this article is available online at: https://doi.org/

Author contributions: CY, TZ, and YB conducted the study design. XY, LZ, and SK provided the observational data. LZ assisted with data processing. CY wrote the manuscript with the help of

TZ and XY. YB, SK, JH, CC, JY, YY, GM, MW, and JC were involved in the scientific interpretation and discussion. All authors provided commentary on the paper.

Competing interests: The authors declare that they have no conflicts of interest.

Acknowledgement: This study was jointly funded by the National Natural Science Foundation of China (41830965; 91744209), the National Key R & D Program Pilot Projects of China (2016YFC0203304), and the Postgraduate Research & Practice Innovation Program of Jiangsu Province (KYCX18_1027).

References

Acciai, C., Zhang, Z., Wang, F., Zhong, Z., and Lonati, G.: Characteristics and source Analysis of trace Elements in $PM_{2.5}$ in the Urban Atmosphere of Wuhan in Spring, Aerosol and Air Quality Research, 17, 2224-2234, https://doi.org/10.4209/aaqr.2017.06.0207, 2017.

An, X., Yao, B., Li, Y., Li, N., and Zhou, L.: Tracking source area of Shangdianzi station using Lagrangian particle dispersion model of FLEXPART, Meteorological Applications, 21, 466-473, https://doi.org/10.1002/met.1358, 2014.

An, Z., Huang, R. J., Zhang, R., Tie, X., Li, G., Cao, J., Zhou, W., Shi, Z., Han, Y., Gu, Z., and Ji, Y.: Severe haze in northern China: A synergy of anthropogenic emissions and atmospheric processes, Proceedings of the National Academy of Sciences, 116, 8657-8666, https://doi.org/10.1073/pnas.1900125116, 2019.

Brioude, J., Arnold, D., Stohl, A., Cassiani, M., Morton, D., Seibert, P., Angevine, W., Evan, S., Dingwell, A., Fast, J. D., Easter, R. C., Pisso, I., Burkhart, J., and Wotawa, G.: The Lagrangian

particle dispersion model FLEXPART-WRF version 3.1, Geoscientific Model Development, 6, 1889-1904, https://doi.org/10.5194/gmd-6-1889-2013, 2013.

Cao, J.-j., Wang, Q.-y., Chow, J. C., Watson, J. G., Tie, X.-x., Shen, Z.-x., Wang, P., and An, Z.-s.: Impacts of aerosol compositions on visibility impairment in Xi'an, China, Atmospheric Environment, 59, 559-566, https://doi.org/10.1016/j.atmosenv.2012.05.036, 2012.

Chang, X., Wang, S., Zhao, B., Cai, S., and Hao, J.: Assessment of inter-city transport of particulate matter in the Beijing-Tianjin-Hebei region, Atmospheric Chemistry and Physics, 18, 4843-4858, https://doi.org/10.5194/acp-18-4843-2018, 2018.

Chen, B., Xu, X.-D., and Zhao, T.: Quantifying oceanic moisture exports to mainland China in association with summer precipitation, Climate Dynamics, 51, 4271-4286, https://doi.org/10.1007/s00382-017-3925-1, 2017a.

Chen, S., Zhou, G., and Zhu, B.: A method for fast quantification of air pollutant sources (in Chinese), Acta Scientiae Circumstantiae, 37, 2474-2481, https://doi.org/10.13671/j.hjkxxb.2017.0045, 2017b.

Cheng, H., Gong, W., Wang, Z., Zhang, F., Wang, X., Lv, X., Liu, J., Fu, X., and Zhang, G.: Ionic composition of submicron particles ($PM_{1.0}$) during the long-lasting haze period in January 2013 in Wuhan, central China, Journal of Environmental Sciences, 26, 810-817, https://doi.org/10.1016/s1001-0742(13)60503-3, 2014.

Cheng, X., Zhao, T., Gong, S., Xu, X., Han, Y., Yin, Y., Tang, L., He, H., and He, J.: Implications of East Asian summer and winter monsoons for interannual aerosol variations over central-eastern China, Atmospheric Environment, 129, 218-228, https://doi.org/10.1016/j.atmosenv.2016.01.037, 2016.

509 Cheng, Y. F., Wiedensohler, A., Eichler, H., Heintzenberg, J., Tesche, M., Ansmann, A., Wendisch,
510 M., Su, H., Althausen, D., and Herrmann, H.: Relative humidity dependence of aerosol optical
511 properties and direct radiative forcing in the surface boundary layer at Xinken in Pearl River Delta
512 of China: An observation based numerical study, Atmospheric Environment, 42, 6373-6397,
513 https://doi.org/10.1016/j.atmosenv.2008.04.009, 2008.
514 Dawson, J., Adams, P., and Pandis, S.: Sensitivity of $PM_{2.5}$ to climate in the Eastern US: a
515 modeling case study, Atmospheric chemistry and physics, 7, 4295-4309,
516 https://doi.org/10.5194/acp-7-4295-2007, 2007.
517 Dawson, J. P., Bloomer, B. J., Winner, D. A., and Weaver, C. P.: Understanding the Meteorological
518 Drivers of U.S. Particulate Matter Concentrations in a Changing Climate, Bulletin of the American
519 Meteorological Society, 95, 521-532, https://doi.org/10.1175/bams-d-12-00181.1, 2014.
520 De Foy, B., Burton, S. P., Ferrare, R. A., Hostetler, C. A., Hair, J. W., Wiedinmyer, C., and Molina,
521 L. T.: Aerosol plume transport and transformation in high spectral resolution lidar measurements
522 and WRF-Flexpart simulations during the MILAGRO Field Campaign, Atmospheric Chemistry
523 and Physics, 11, 3543-3563, https://doi.org/10.5194/acp-11-3543-2011, 2011.
524 Deng, J., Wang, T., Jiang, Z., Xie, M., Zhang, R., Huang, X., and Zhu, J.: Characterization of
525 visibility and its affecting factors over Nanjing, China, Atmospheric Research, 101, 681-691,
526 https://doi.org/10.1016/j.atmosres.2011.04.016, 2011.
527 Ding, A., Wang, T., Xue, L., Gao, J., Stohl, A., Lei, H., Jin, D., Ren, Y., Wang, X., and Wei, X.:
528 Transport of north China air pollution by midlatitude cyclones: Case study of aircraft
529 measurements in summer 2007, Journal of Geophysical Research: Atmospheres, 114,
530 https://doi.org/doi:10.1029/2008JD011023, 2009.

Ding, Y.: Monsoons over china, Springer Science & Business Media, 1993.

Ding, Y., Wu, P., Liu, Y., and Song, Y.: Environmental and Dynamic Conditions for the Occurrence of Persistent Haze Events in North China, Engineering, 3, 266-271, https://doi.org/10.1016/j.eng.2017.01.009, 2017.

Fast, J. D., and Easter, R. C.: A Lagrangian particle dispersion model compatible with WRF, 7th WRF Users Workshop, NCAR, 2006, 19-22.

Fuzzi, S., Baltensperger, U., Carslaw, K., Decesari, S., Denier van der Gon, H., Facchini, M. C., Fowler, D., Koren, I., Langford, B., Lohmann, U., Nemitz, E., Pandis, S., Riipinen, I., Rudich, Y., Schaap, M., Slowik, J. G., Spracklen, D. V., Vignati, E., Wild, M., Williams, M., and Gilardoni, S.: Particulate matter, air quality and climate: lessons learned and future needs, Atmospheric Chemistry and Physics, 15, 8217-8299, https://doi.org/10.5194/acp-15-8217-2015, 2015.

Gao, Y., X. Liu, C. Zhao, and M. Zhang.: Emission controls versus meteorological conditions in determining aerosol concentrations in Beijing during the 2008 Olympic Games, Atmospheric Chemistry and Physics, 11, 12437-12451, https://doi.org/10.5194/acp-11-12437-2011, 2011.

Gong, W., Zhang, T., Zhu, Z., Ma, Y., Ma, X., and Wang, W.: Characteristics of $PM_{1.0}$, $PM_{2.5,}$ and PM_{10}, and Their Relation to Black Carbon in Wuhan, Central China, Atmosphere, 6, 1377-1387, https://doi.org/10.3390/atmos6091377, 2015.

Grell, G. A., Peckham, S. E., Schmitz, R., McKeen, S. A., Frost, G., Skamarock, W. C., and Eder, B.: Fully coupled “online” chemistry within the WRF model, Atmospheric Environment, 39, 6957-6975, https://doi.org/10.1016/j.atmosenv.2005.04.027, 2005.

He, J., Mao, H., Gong, S., Yu, Y., Wu, L., Liu, H., Chen, Y., Jing, B., Ren, P., and Zou, C.: Investigation of Particulate Matter Regional Transport in Beijing Based on Numerical Simulation,

553 Aerosol and Air Quality Research, 17, 1181-1189, https://doi.org/10.4209/aaqr.2016.03.0110,
554 2017.
555 He, K., Zhao, Q., Ma, Y., Duan, F., Yang, F., Shi, Z., and Chen, G.: Spatial and seasonal variability
556 of $PM_{2.5}$ acidity at two Chinese megacities: insights into the formation of secondary inorganic
557 aerosols, Atmospheric Chemistry and Physics, 12, 1377-1395,
558 https://doi.org/10.5194/acp-12-1377-2012, 2012.
559 Hong, S.-Y., Noh, Y., and Dudhia, J.: A new vertical diffusion package with an explicit treatment
560 of entrainment processes, Monthly weather review, 134, 2318-2341,
561 https://doi.org/10.1175/MWR3199.1,2006, 2006.
562 Hu, J., Li, Y., Zhao, T., Liu, J., Hu, X.-M., Liu, D., Jiang, Y., Xu, J., and Chang, L.: An important
563 mechanism of regional O_3 transport for summer smog over the Yangtze River Delta in eastern
564 China, Atmospheric Chemistry and Physics, 18, 16239-16251,
565 https://doi.org/10.5194/acp-18-16239-2018, 2018.
566 Huang, Q., Cai, X., Wang, J., Song, Y., and Zhu, T.: Climatological study of the Boundary-layer
567 air Stagnation Index for China and its relationship with air pollution, Atmospheric Chemistry and
568 Physics, 18, 7573-7593, https://doi.org/10.5194/acp-18-7573-2018, 2018.
569 Huang, R. J., Zhang, Y., Bozzetti, C., Ho, K. F., Cao, J. J., Han, Y., Daellenbach, K. R., Slowik, J.
570 G., Platt, S. M., Canonaco, F., Zotter, P., Wolf, R., Pieber, S. M., Bruns, E. A., Crippa, M., Ciarelli,
571 G., Piazzalunga, A., Schwikowski, M., Abbaszade, G., Schnelle-Kreis, J., Zimmermann, R., An, Z.,
572 Szidat, S., Baltensperger, U., El Haddad, I., and Prevot, A. S.: High secondary aerosol contribution
573 to particulate pollution during haze events in China, Nature, 514, 218-222,
574 https://doi.org/10.1038/nature13774, 2014.

575 Jiang, C., Wang, H., Zhao, T., Li, T., and Che, H.: Modeling study of $PM_{2.5}$ pollutant transport
576 across cities in China's Jing-Jin-Ji region during a severe haze episode in December 2013,
577 Atmospheric Chemistry and Physics, 15, 5803-5814, https://doi.org/10.5194/acp-15-5803-2015,
578 2015.
579 Kang, H., Zhu, B., Gao, J., He, Y., Wang, H., Su, J., Pan, C., Zhu, T., and Yu, B.: Potential impacts
580 of cold frontal passage on air quality over the Yangtze River Delta, China, Atmospheric Chemistry
581 and Physics, 19, 3673-3685, https://doi.org/10.5194/acp-19-3673-2019, 2019.
582 Miao, Y., Guo, J., Liu, S., Zhao, C., Li, X., Zhang, G., Wei, W., and Ma, Y.: Impacts of synoptic
583 condition and planetary boundary layer structure on the trans-boundary aerosol transport from
584 Beijing-Tianjin-Hebei region to northeast China, Atmospheric Environment, 181, 1-11,
585 https://doi.org/10.1016/j.atmosenv.2018.03.005, 2018.
586 Mlawer, E. J., Taubman, S. J., Brown, P. D., Iacono, M. J., and Clough, S. A.: Radiative transfer
587 for inhomogeneous atmospheres: RRTM, a validated correlated-k model for the longwave, Journal
588 of Geophysical Research: Atmospheres, 102, 16663-16682, https://doi.org/10.1029/97jd00237,
589 1997.
590 Morrison, H., Thompson, G., and Tatarskii, V.: Impact of Cloud Microphysics on the Development
591 of Trailing Stratiform Precipitation in a Simulated Squall Line: Comparison of One- and
592 Two-Moment Schemes, Monthly Weather Review, 137, 991-1007,
593 https://doi.org/10.1175/2008mwr2556.1, 2009.
594 Nel, A.: Air pollution-related illness: effects of particles, Science, 308, 804-806,
595 https://doi.org/10.1126/science.1108752, 2005.
596 Oke, T. R.: Boundary layer climates, Routledge, 2002.

597 Qiao, X., Guo, H., Tang, Y., Wang, P., Deng, W., Zhao, X., Hu, J., Ying, Q., and Zhang, H.: Local
598 and regional contributions to fine particulate matter in the 18 cities of Sichuan Basin, southwestern
599 China, Atmospheric Chemistry and Physics, 19, 5791-5803,
600 https://doi.org/10.5194/acp-19-5791-2019, 2019.
601 Sauvage, B., Fontaine, A., Eckhardt, S., Auby, A., Boulanger, D., Petetin, H., Paugam, R., Athier,
602 G., Cousin, J.-M., Darras, S., Nédélec, P., Stohl, A., Turquety, S., Cammas, J.-P., and Thouret, V.:
603 Source attribution using FLEXPART and carbon monoxide emission inventories: SOFT-IO
604 version 1.0, Atmospheric Chemistry and Physics, 17, 15271-15292,
605 https://doi.org/10.5194/acp-17-15271-2017, 2017.
606 Seibert, P., and Frank, A.: Source-receptor matrix calculation with a Lagrangian particle dispersion
607 model in backward mode, Atmospheric Chemistry and Physics, 4, 51-63,
608 https://doi.org/10.5194/acp-4-51-2004, 2004.
609 Stohl, A., Forster, C., Eckhardt, S., Spichtinger, N., Huntrieser, H., Heland, J., Schlager, H.,
610 Wilhelm, S., Arnold, F., and Cooper, O.: A backward modeling study of intercontinental pollution
611 transport using aircraft measurements, Journal of Geophysical Research: Atmospheres, 108,
612 https://doi.org/10.1029/2002jd002862, 2003.
613 Stohl, A., Forster, C., Frank, A., Seibert, P., and Wotawa, G.: Technical note: The Lagrangian
614 particle dispersion model FLEXPART version 6.2, Atmospheric Chemistry & Physics, 5,
615 2461-2474, https://doi.org/10.5194/acp-5-2461-2005, 2005.
616 Taylor, K. E.: Summarizing multiple aspects of model performance in a single diagram, Journal of
617 Geophysical Research: Atmospheres, 106, 7183-7192, https://doi.org/10.1029/2000jd900719,
618 2001.

619 Tie, X., Huang, R. J., Cao, J., Zhang, Q., Cheng, Y., Su, H., Chang, D., Poschl, U., Hoffmann, T.,
620 Dusek, U., Li, G., Worsnop, D. R., and O'Dowd, C. D.: Severe Pollution in China Amplified by
621 Atmospheric Moisture, Science Report, 7, 15760, https://doi.org/10.1038/s41598-017-15909-1,
622 2017.
623 Voulgarakis, A., Savage, N., Wild, O., Braesicke, P., Young, P., Carver, G., and Pyle, J.:
624 Interannual variability of tropospheric composition: the influence of changes in emissions,
625 meteorology and clouds, Atmospheric Chemistry and Physics, 10, 2491-2506,
626 https://doi.org/10.5194/acp-10-2491-2010, 2010.
627 Wang, H. L., Qiao, L. P., Lou, S. R., Zhou, M., Ding, A. J., Huang, H. Y., Chen, J. M., Wang, Q.,
628 Tao, S. K., Chen, C. H., Li, L., and Huang, C.: Chemical composition of $PM_{2.5}$ and meteorological
629 impact among three years in urban Shanghai, China, Journal of Cleaner Production, 112,
630 1302-1311, https://doi.org/10.1016/j.jclepro.2015.04.099, 2016.
631 Wang, S. X., Zhao, B., Cai, S. Y., Klimont, Z., Nielsen, C. P., Morikawa, T., Woo, J. H., Kim, Y.,
632 Fu, X., Xu, J. Y., Hao, J. M., and He, K. B.: Emission trends and mitigation options for air
633 pollutants in East Asia, Atmospheric Chemistry and Physics, 14, 6571-6603,
634 https://doi.org/10.5194/acp-14-6571-2014, 2014.
635 Wu, J., Kong, S., Wu, F., Cheng, Y., Zheng, S., Yan, Q., Zheng, H., Yang, G., Zheng, M., Liu, D.,
636 Zhao, D., and Qi, S.: Estimating the open biomass burning emissions in central and eastern China
637 from 2003 to 2015 based on satellite observation, Atmospheric Chemistry and Physics, 18,
638 11623-11646, https://doi.org/10.5194/acp-18-11623-2018, 2018.
639 Xu, G., Jiao, L., Zhang, B., Zhao, S., Yuan, M., Gu, Y., Liu, J., and Tang, X.: Spatial and Temporal
640 Variability of the $PM_{2.5}/PM_{10}$ Ratio in Wuhan, Central China, Aerosol and Air Quality Research,

17, 741-751, https://doi.org/10.4209/aaqr.2016.09.0406, 2017.

Xu, J., Chang, L., Qu, Y., Yan, F., Wang, F., and Fu, Q.: The meteorological modulation on $PM_{2.5}$ interannual oscillation during 2013 to 2015 in Shanghai, China, Science of the Total Environment, 572, 1138-1149, https://doi.org/10.1016/j.scitotenv.2016.08.024, 2016a.

Xu, X., Zhao, T., Liu, F., Gong, S. L., Kristovich, D., Lu, C., Guo, Y., Cheng, X., Wang, Y., and Ding, G.: Climate modulation of the Tibetan Plateau on haze in China, Atmospheric Chemistry and Physics, 16, 1365-1375, https://doi.org/10.5194/acp-16-1365-2016, 2016b.

Zhai, S., An, X., Liu, Z., Sun, Z., and Hou, Q.: Model assessment of atmospheric pollution control schemes for critical emission regions, Atmospheric Environment, 124, 367-377, https://doi.org/10.1016/j.atmosenv.2015.08.093, 2016.

Zhang, F., Wang, Z. W., Cheng, H. R., Lv, X. P., Gong, W., Wang, X. M., and Zhang, G.: Seasonal variations and chemical characteristics of $PM_{2.5}$ in Wuhan, central China, Science of the Total Environment, 518-519, 97-105, https://doi.org/10.1016/j.scitotenv.2015.02.054, 2015.

Zhang, R., Li, Q., and Zhang, R.: Meteorological conditions for the persistent severe fog and haze event over eastern China in January 2013, Science China Earth Sciences, 57, 26-35, https://doi.org/10.1007/s11430-013-4774-3, 2013.

Zhang, X. Y., Wang, Y. Q., Niu, T., Zhang, X. C., Gong, S. L., Zhang, Y. M., and Sun, J. Y.: Atmospheric aerosol compositions in China: spatial/temporal variability, chemical signature, regional haze distribution and comparisons with global aerosols, Atmospheric Chemistry and Physics, 12, 779-799, https://doi.org/10.5194/acp-12-779-2012, 2012.

Zhao, T., Gong, S., Huang, P., and Lavoué, D.: Hemispheric transport and influence of meteorology on global aerosol climatology, Atmospheric Chemistry & Physics Discussions, 12,

https://doi.org/10.5194/acp-12-7609-2012, 2012.

Zhao, X. J., Zhao, P. S., Xu, J., Meng, W., Pu, W. W., Dong, F., He, D., and Shi, Q. F.: Analysis of a winter regional haze event and its formation mechanism in the North China Plain, Atmospheric Chemistry and Physics, 13, 5685-5696, https://doi.org/10.5194/acp-13-5685-2013, 2013.

Zheng, H., Kong, S., Wu, F., Cheng, Y., Niu, Z., Zheng, S., Yang, G., Yao, L., Yan, Q., Wu, J., Zheng, M., Chen, N., Xu, K., Yan, Y., Liu, D., Zhao, D., Zhao, T., Bai, Y., Li, S., and Qi, S.: Intra-regional transport of black carbon between the south edge of the North China Plain and central China during winter haze episodes, Atmospheric Chemistry and Physics, 19, 4499-4516, https://doi.org/10.5194/acp-19-4499-2019, 2019.

Zhong, J., Zhang, X., Wang, Y., Wang, J., Shen, X., Zhang, H., Wang, T., Xie, Z., Liu, C., Zhang, H., Zhao, T., Sun, J., Fan, S., Gao, Z., Li, Y., and Wang, L.: The two-way feedback mechanism between unfavorable meteorological conditions and cumulative aerosol pollution in various haze regions of China, Atmos. Chem. Phys., 19, 3287–3306, https://doi.org/10.5194/acp-19-3287-2019, 2019.

677 **Table 1.** Correlation coefficients between hourly $PM_{2.5}$ concentrations and near-surface
678 meteorological elements WS (wind speed), T (air temperature), P (air pressure), and RH (relative
679 humidity) in Wuhan in January 2016.

Correlation coefficients	WS	T	P	RH
$PM_{2.5}$	0.10	0.31	-0.47	0.20

680 **Table 2.** Correlation coefficients of $PM_{2.5}$ concentrations with wind speed (WS) and air
681 temperature (T) in different air quality levels during the study period.

Air quality	$PM_{2.5}$ levels	Number of samples	WS	T
Clean	$PM_{2.5}$ <75 μg m^{-3}	73	-0.20	0.56
Light pollution	75 μg m^{-3}≤ $PM_{2.5}$ <150 μg m^{-3}	135	-0.19	0.15
Heavy pollution	$PM_{2.5}$ ≥150 μg m^{-3}	37	0.41	-0.08

682

683 **Table 3.** Atmospheric static stability below heights of 200 m in the boundary layer during heavy
684 pollution and clean air periods with anomalies relative to the average over January 2016 in
685 Wuhan.

Period	heavy pollution period	clean air period	monthly average
	(K km^{-1})	(K km^{-1})	(K km^{-1})
Static stability	4.4	13.2	8.6
Anomalies of stability	-4.2	4.6	-

686

687 **Table 4.** The relative contributions of regional transport over CEC to three $PM_{2.5}$ heavy pollution

688 periods, P1, P2, and P3, in the YRMB with local contributions.

Contribution rates	P1	P2	P3	Averages
Regional transport	68.1%	60.9%	65.3%	65.1%
Local contribution	31.9%	39.1%	34.7%	34.9%

689

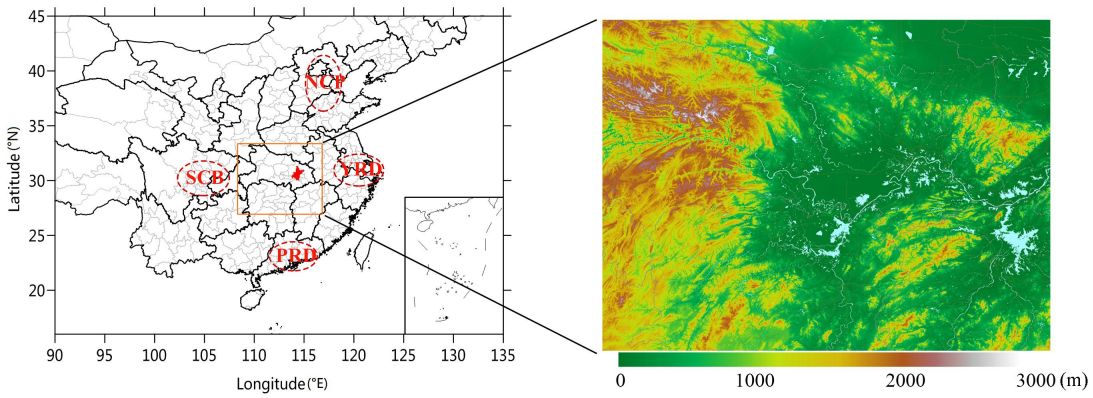

690

691 **Fig. 1.** (a) Distribution of the YRMB (orange rectangle) with the location of Wuhan (red area) and

692 the major haze pollution regions of NCP, YRD, PRD, and SCB in CEC as well as (b) the YRMB

693 region with terrain height (color contours, m in a.s.l.). The river and lake network (blue areas) are

694 downloaded from https://worldview.earthdata.nasa.gov.

695

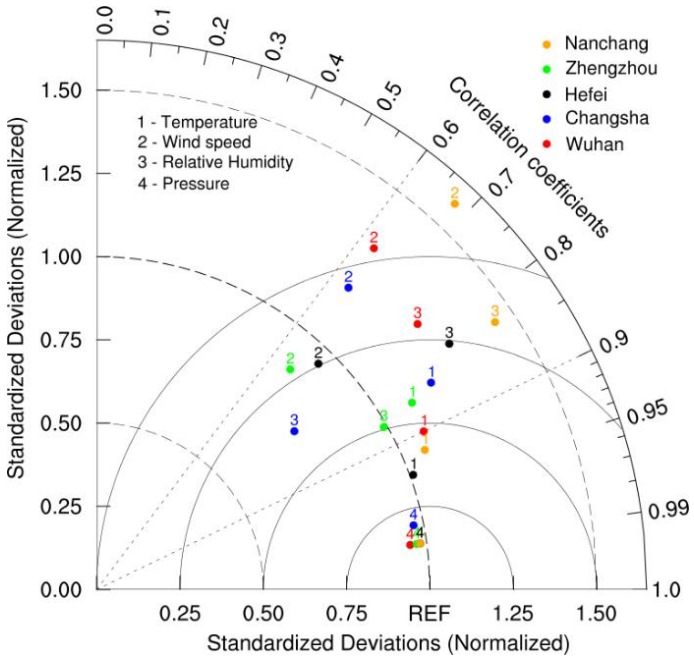

696

697 **Fig. 2.** A Taylor plot with the normalized standard deviations and correlation coefficients between

698 WRF-simulated and observed meteorological fields. The radian of the sector represents the

699 correlation coefficient. The solid line indicates the ratio of standard deviation between simulations

and observations. The distance from the marker to "REF" reflect the normalized root-mean-square error (NRMSE).

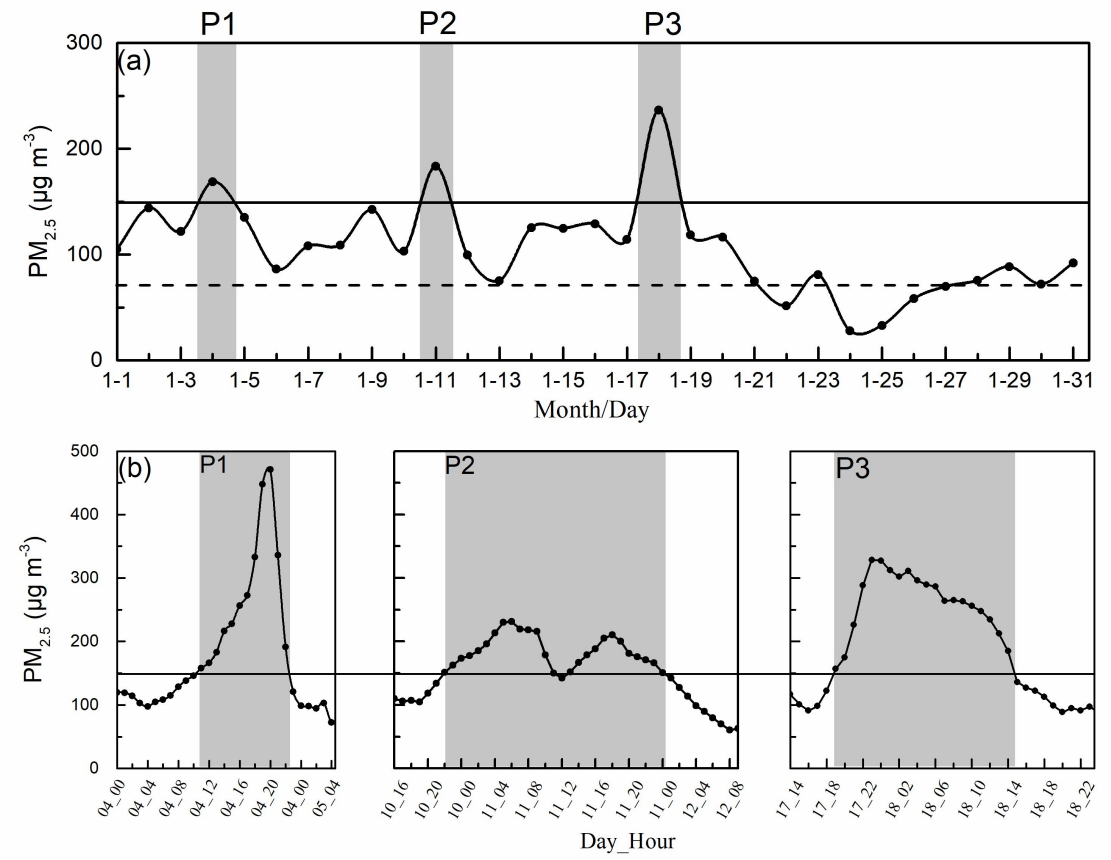

Fig. 3. (a) Daily changes of surface $PM_{2.5}$ concentrations in Wuhan in January 2016 with $PM_{2.5}$ concentrations exceeding 75 μg m^{-3} (dash line) and 150 μg m^{-3} (solid lines) for light and heavy haze pollution, respectively. (b) The hourly variations of surface $PM_{2.5}$ concentrations in three heavy air pollution events, P1, P2, and P3, with excessive $PM_{2.5}$ levels (> 150 μg m^{-3}) marked by the shaded areas.

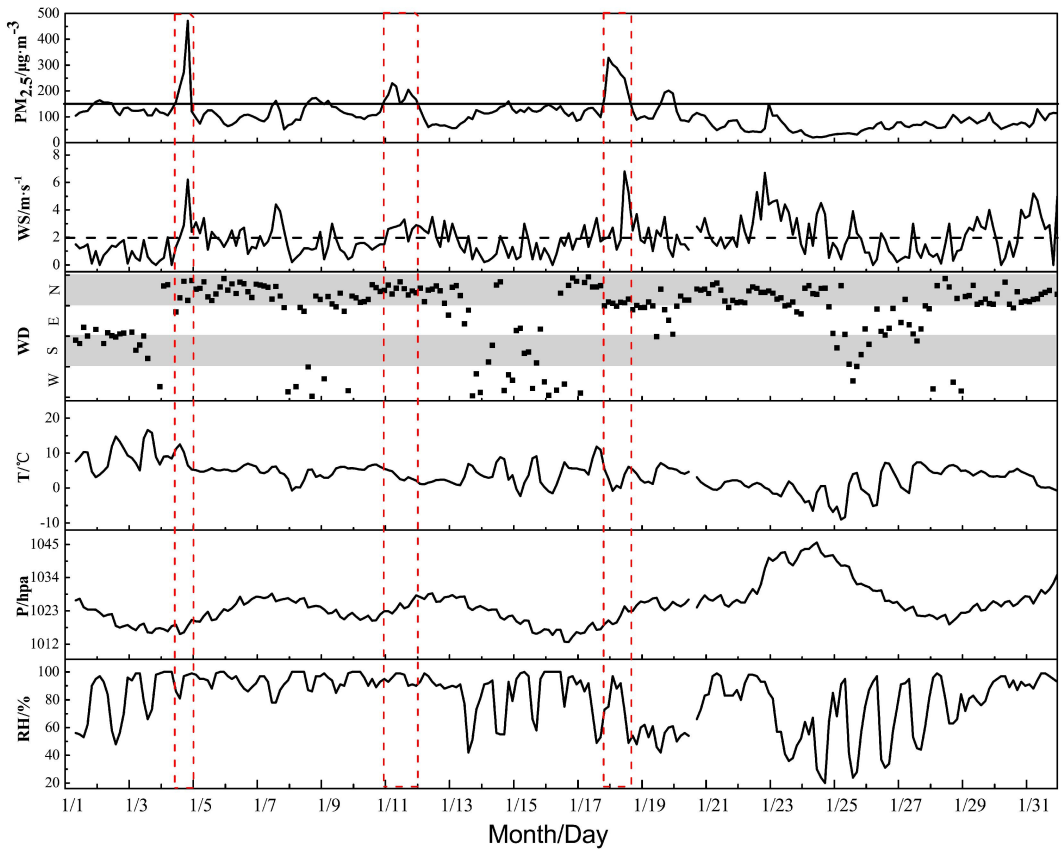

710

711 **Fig. 4.** Hourly variations of meteorological elements and $PM_{2.5}$ concentrations in Wuhan in

712 January 2016. Heavy air pollution periods are marked with columns in red dash lines and $PM_{2.5}$

713 concentrations exceeding 150 μg m^{-3} (solid line in the upper panel).

714

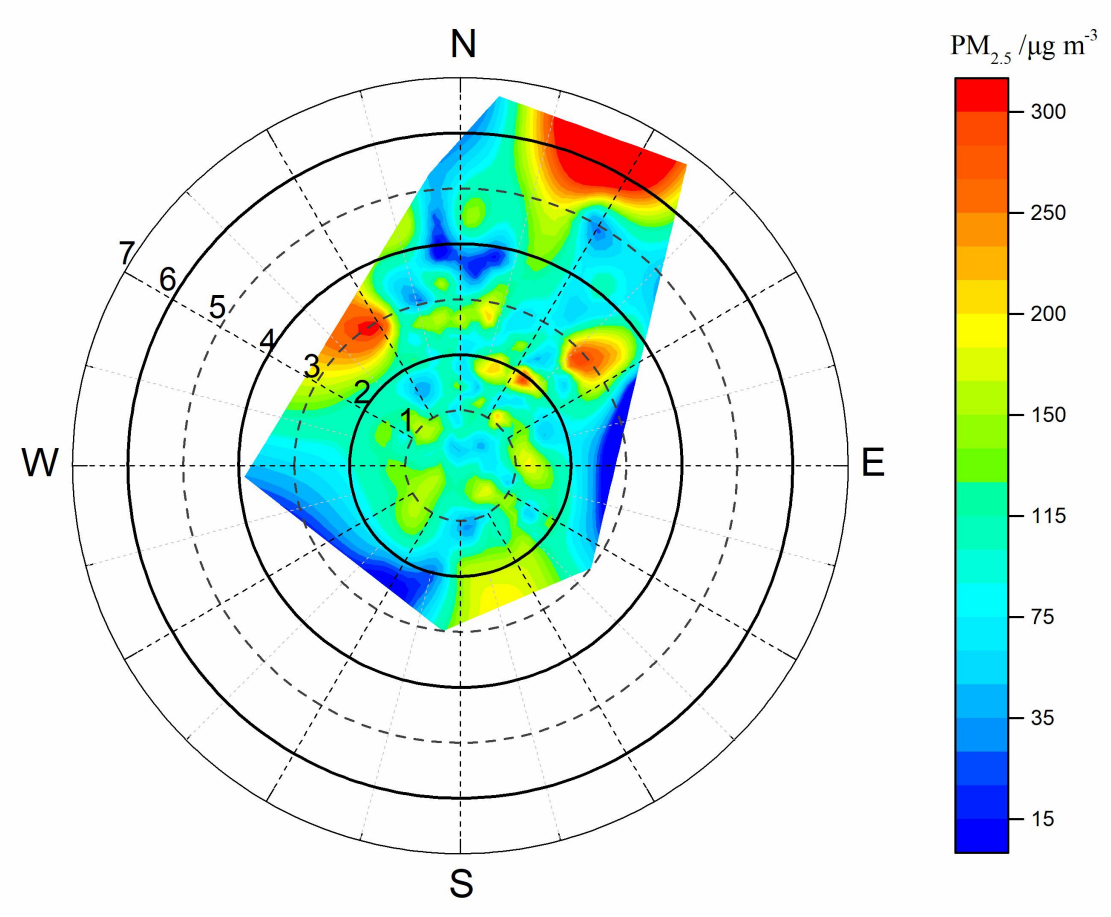

715

716 **Fig. 5.** A polar plot of the hourly variations in wind speed (round radius, in units of m s^{-1}) and

717 direction (angles) to surface $PM_{2.5}$ concentrations (color contours, in units of μg m^{-3}) in Wuhan in

718 January 2016.

719

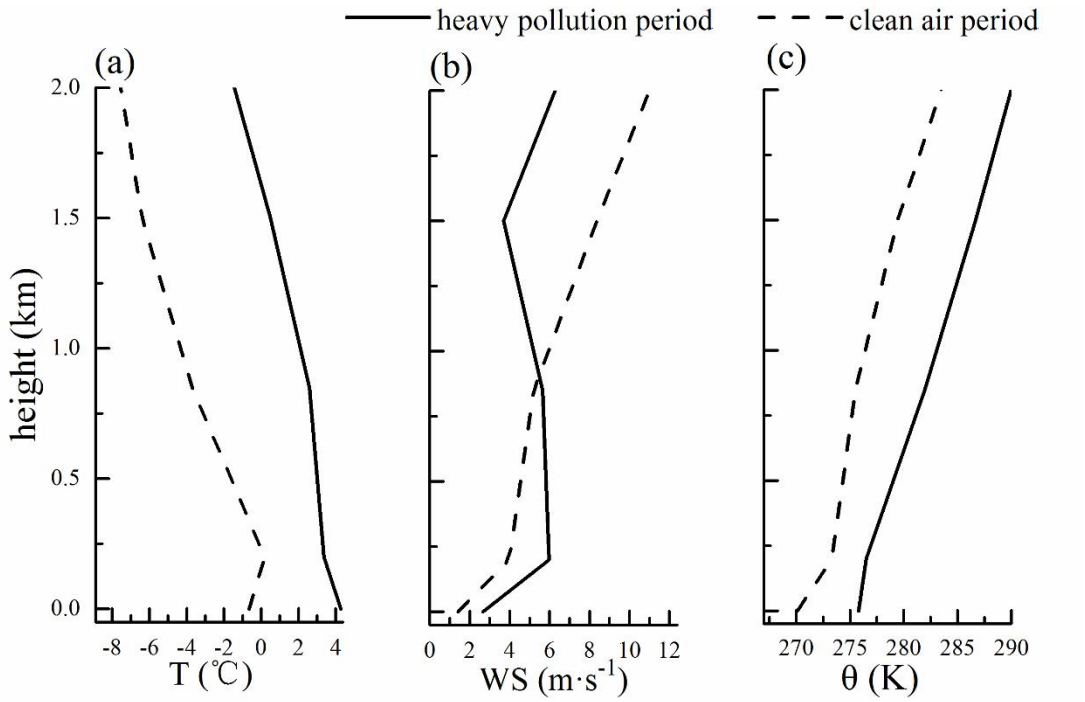

720

721 **Fig. 6.** Vertical profiles of (a) air temperature, (b) wind velocity and (c) potential temperature

722 averaged in the heavy pollution periods P1, P2 and P3 and in the clean air period over Wuhan

723 during January 2016.

724

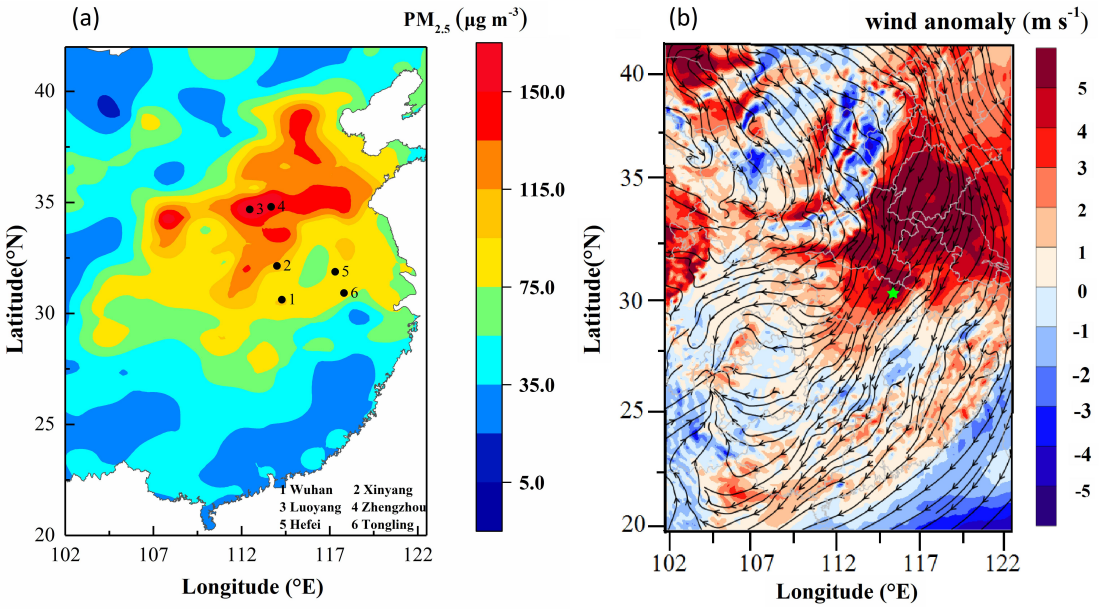

725

726 **Fig. 7** (a) Distribution of the monthly averages of surface $PM_{2.5}$ concentrations observed in

January 2016 over CEC with the locations of six sites (black dots): 1. Wuhan, 2. Xinyang, 3. Luoyang, 4. Zhengzhou, 5. Hefei, and 6. Tongling. (b) Distribution of anomalies (color contours) of 200 m wind speeds averaged during the three heavy air pollution periods relative to the monthly wind averages (streamlines) in January 2016 over CEC with the location of Wuhan (a light blue star).

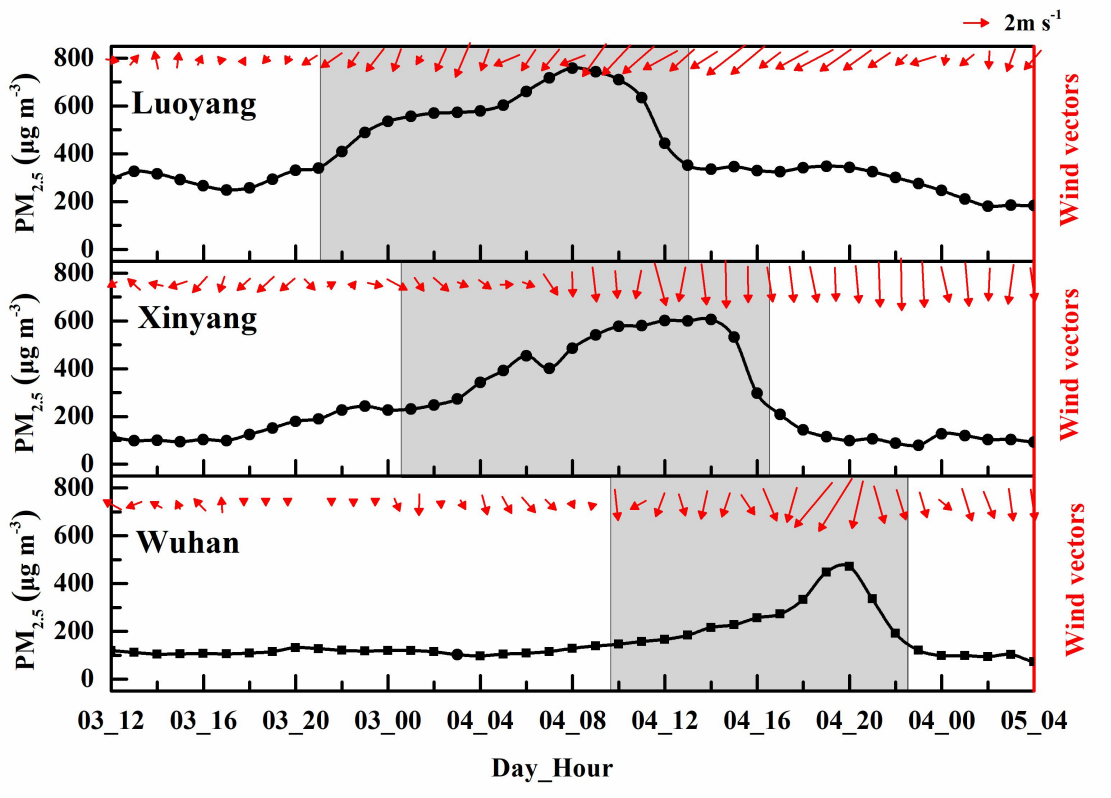

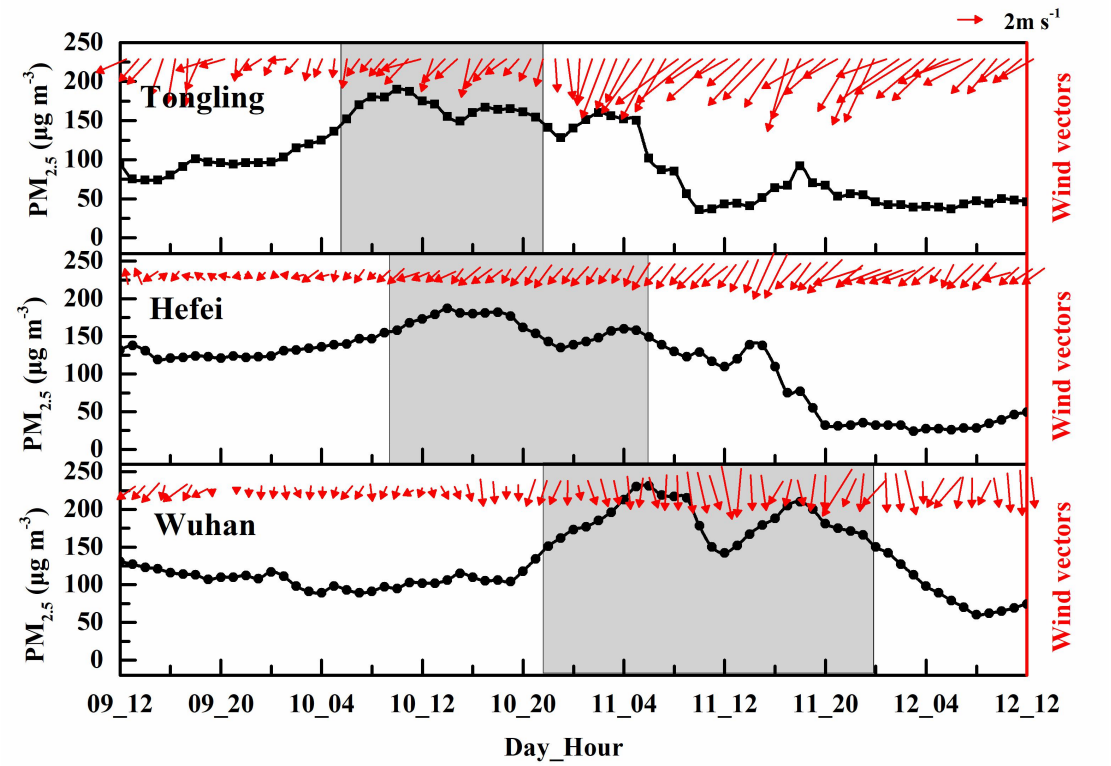

734

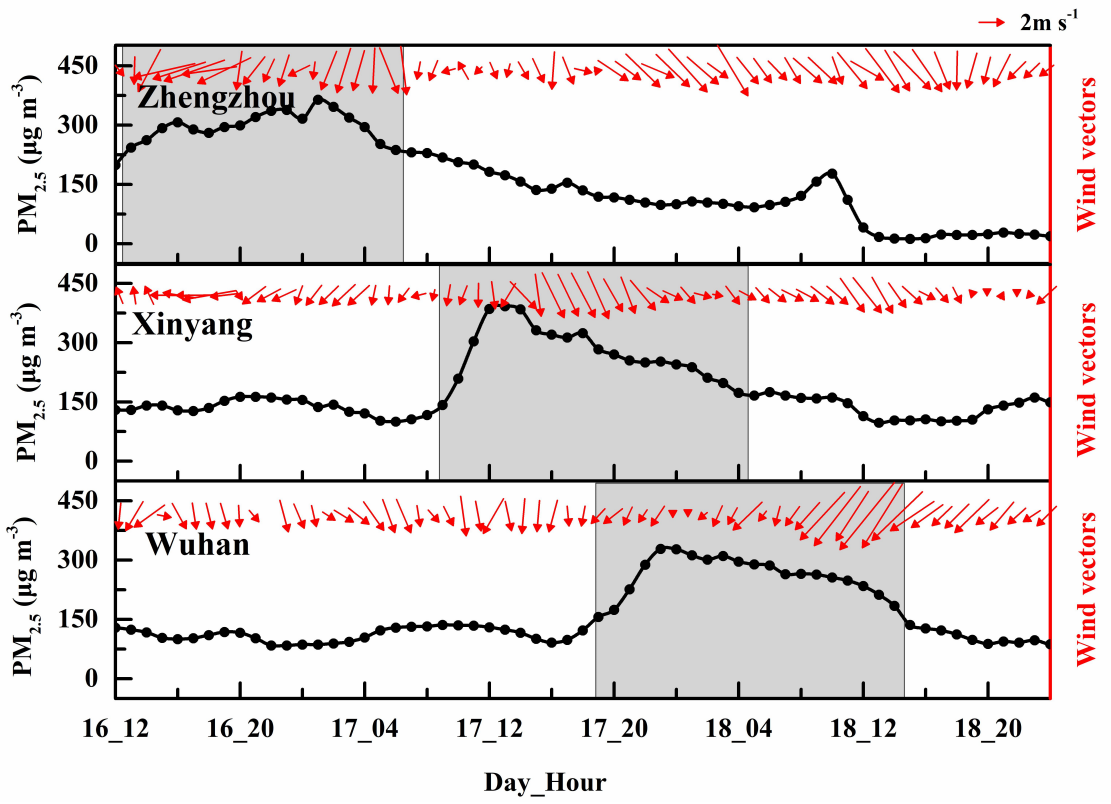

735

736 **Fig. 8.** Temporal changes of $PM_{2.5}$ concentrations (dotted lines) and near-surface winds (vectors)

737 observed at five upstream sites (Fig. 6) and Wuhan with shifts of $PM_{2.5}$ peaks (marked with shaded

738 areas) to the YRMB's heavy $PM_{2.5}$ pollution periods P1 (upper panel), P2 (middle panel) and P3

739 (lower panel), in January 2016.

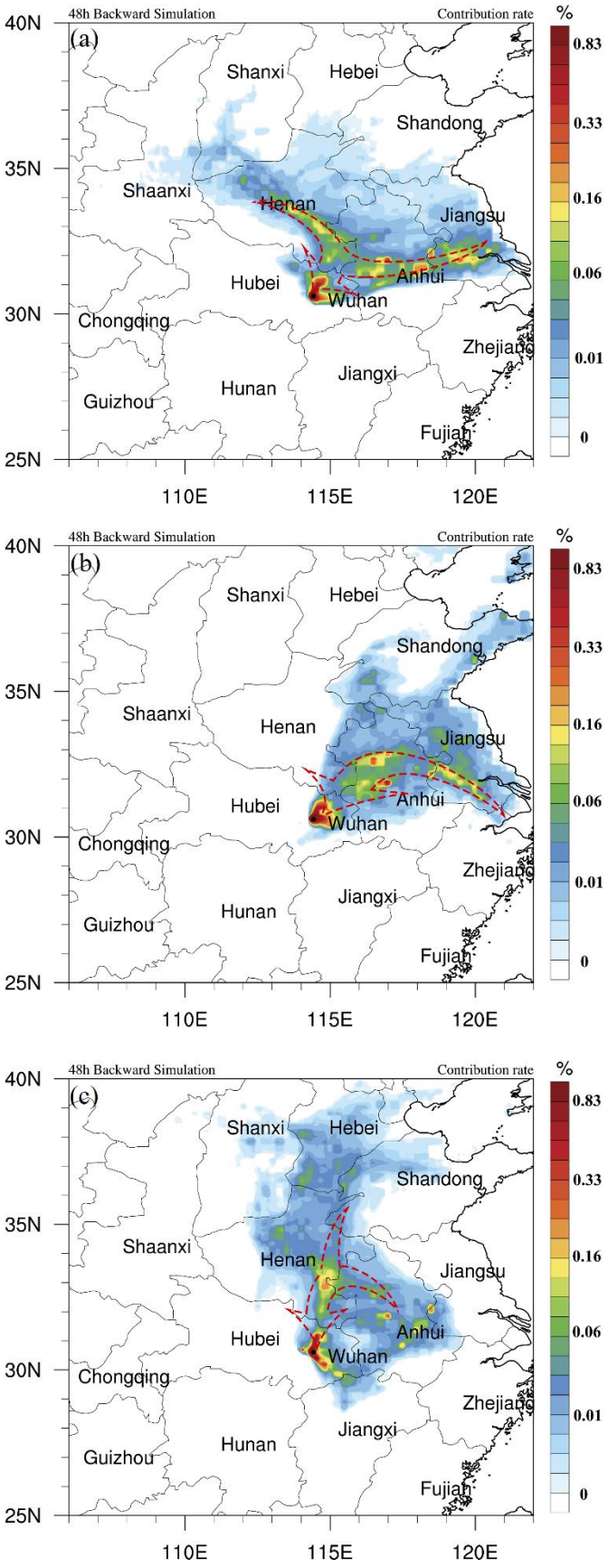

740

741 **Fig. 9.** Spatial distribution of contribution rates (color contours) to $PM_{2.5}$ concentrations in Wuhan

with the major pathways of regional transport over CEC (dash arrows) for three heavy pollution periods (a) P1, (b) P2, and (c) P3 in January 2016 simulated by the FLEXPART-WRF model.